

A deconvolution inverse scattering imaging condition for RTM separated wavefield imaging

Sean Crawley, Elena Klochikhina, and Dan Whitmore, PGS.

Summary

We describe a new imaging condition for reverse-time migration (RTM). Specifically, we extend the inverse scattering imaging condition (ISIC) to deconvolution in the temporal frequency domain, and apply it in an RTM version of Separated Wavefield Imaging (SWIM). Tests on both synthetic and field data show this method successfully removes low-wavenumber artifacts associated with backscattered energy and has similar strengths and challenges to deconvolution-based SWIM with one-way wave equation migration.

Introduction

Wave equation imaging of primaries, whether with a one-way (WEM) or two-way wave equation (RTM), is typically done by cross correlating a synthetic source wavefield propagated forward and a recorded receiver wavefield propagated backward. The spectrum of the source wavefield can be specified to get the desired character in the image.

In SWIM, both the source and receiver wavefields are made from recorded data. This has the benefit that every receiver becomes a virtual source. Since receivers are typically much denser than sources, migrating the multiples potentially enhances subsurface illumination and resolution (Valenciano et al., 2014). However, it also means the cross-correlation image contains the data's source wavelet squared. It tends to be narrow in wavenumber, and prone to reverberation in depth.

A deconvolution-based imaging condition is preferable to cross correlation in the case of SWIM because it fixes this issue. The wavelet is deconvolved so the image spectrum tends to be flat. A deconvolution imaging condition is straightforward to implement for WEM (Whitmore et al., 2010), but requires some changes for RTM.

In RTM (at least in 3D), it is more difficult to implement a deconvolution imaging condition in a practical way because of the memory required. We use domain decomposition to spread the memory among compute nodes, enabling the same deconvolution imaging condition used for SWIM in WEM to be used in RTM.

RTM images, whether conventional or SWIM, and whether formed with cross-correlation or deconvolution, are prone to low-wavenumber backscattering artifacts (Yoon et al., 2004; Poole et al., 2010). An inverse scattering imaging condition (ISIC) is one method to eliminate these artifacts

from correlation-based RTM images (Stolk et al., 2009; Wang et al., 2010; Whitmore and Crawley, 2012). We extend ISIC from cross correlation in time to deconvolution in temporal frequency and produce SWIM RTM images with enhanced resolution and spectral character, and with reduced backscattering artifacts.

Method

ISIC, described by equations 1-3, produces RTM images without low-wavenumber artifacts. It consists of a weighted sum of two image kernels, each combining the forward- and backward-propagated wavefields: the dot product of the gradients and the cross correlation of the time derivatives. These kernels correspond to equations 2 and 3 below. Variables S and R are the source (forward) and receiver (backward) wavefields, v and ω are the velocity and frequency, and W_1 and W_2 are weights that are adaptively determined functions of time and space.

$$I(\bar{x}) = \int [W_1(\bar{x}, t)J_1(\bar{x}, t) + W_2(\bar{x}, t)J_2(\bar{x}, t)] dt \quad (1)$$

$$J_1(\bar{x}, t) = \frac{v^2}{\omega^2} [\nabla R(\bar{x}, T - t) \cdot \nabla S(\bar{x}, t)] \quad (2)$$

$$J_2(\bar{x}, t) = \frac{1}{\omega^2} \left[\frac{\partial}{\partial t} R(\bar{x}, T - t) \cdot \frac{\partial}{\partial t} S(\bar{x}, t) \right] \quad (3)$$

Figures 1a and 1b show an example of each kernel for the migration of a single seismic trace acquired over a two-layer model. Figure 1a shows the time derivative image, and 1b the gradient image. Figure 1c shows the migration result from the weighted combination of the two, containing the migration isochron but not the backscattering “rabbit ear” artifact. The isochron is similar in both image kernels, but the artifact is out of phase and cancels out in the sum.

Equations 1-3 are good for imaging primaries, but for SWIM we would prefer a deconvolution imaging condition (Whitmore et al., 2010), like the one shown in Equation 4.

$$I(\bar{x}) = \int \frac{S^*(\bar{x}, \omega)R(\bar{x}, \omega)}{\langle S(\bar{x}, \omega)S^*(\bar{x}, \omega) \rangle + \varepsilon(\bar{x}, \omega)} d\omega \quad (4)$$

Here the angle brackets in the denominator stand for smoothing in the spatial directions (Guitton et al., 2007), and ε is a damping factor. Equation 4 is straightforward to implement for one-way wave equation migration (though exactly how to smooth and damp are serious practical issues). Those methods naturally work one (or a few)

Deconvolution ISIC

frequencies and depths at a time, so the wavefields S and R do not require much memory.

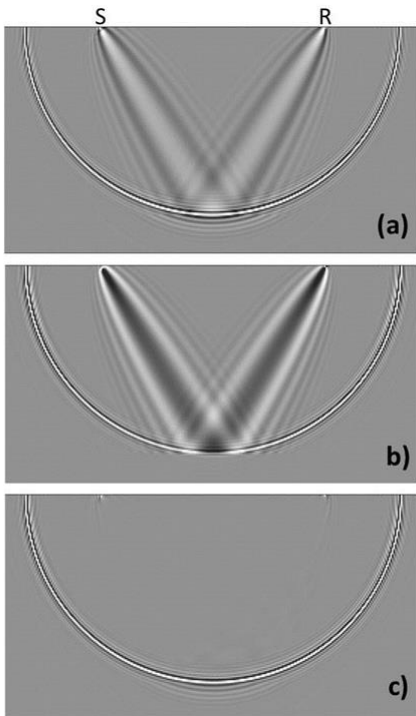


Figure 1: ISIC in RTM. (a) Time derivative image kernel, (b) gradient kernel, and (c) migrated image (weighted sum of a and b). Locations of the source and receiver are also shown.

In RTM, the wavefields propagate through time, at all (x,y,z) simultaneously. They naturally occur as $f(z,x,y,t)$ and are typically too large to be stored in the memory of a single node. This makes Fourier transforming the outer axis, and getting $S(z,x,y,\omega)$ and $R(z,x,y,\omega)$ to form the deconvolution image, problematic. We implement equation 4 by decomposing the calculation of S and R across multiple nodes. Each node holds a subset of the spatial axes, but the entire range of times t in memory, so that Fourier transforming t to ω is easy.

To remove backscatter artifacts from the resulting images, we split equation 4 into pieces, similar to equations 1-3:

$$I(\bar{x}) = \int [W_1(\bar{x}, \omega)J_1(\bar{x}, \omega) + W_2(\bar{x}, \omega)J_2(\bar{x}, \omega)] d\omega \quad (5)$$

$$J_1(\bar{x}, \omega) = \frac{\frac{v^2}{\omega^2} [\nabla R(\bar{x}, \omega) \cdot \nabla S(\bar{x}, \omega)]}{\langle S(\bar{x}, \omega)S^*(\bar{x}, \omega) \rangle + \varepsilon(\bar{x}, \omega)} \quad (6)$$

$$J_2(\bar{x}, \omega) = \frac{\frac{1}{\omega^2} [\frac{\partial}{\partial t} R(\bar{x}, \omega) \cdot \frac{\partial}{\partial t} S(\bar{x}, \omega)]}{\langle S(\bar{x}, \omega)S^*(\bar{x}, \omega) \rangle + \varepsilon(\bar{x}, \omega)} \quad (7)$$

Equations 5-7 work much like equations 1-3. Again the image is a weighted sum of two imaging kernels, one with derivatives in time and one in space. But now they are deconvolved and stacked over frequencies rather than times. The weighting functions W are still determined adaptively, but are now functions of space and frequency.

Synthetic example

Figures 2, 3, and 4 show deconvolution ISIC applied to a version of the 2D Sigsbee synthetic data, modeled with free surface multiples. Figure 2 shows a zoomed-in portion of the gradient kernel from equation 6, and Figure 3 shows the time derivative kernel from equation 7. These images are dominated by low-wavenumber artifacts from the top of the salt. The weighted sum of the two images produces the image shown in Figure 4, without wavenumber filters or additional processing. SWIM produces a clear image without backscattering artifacts.

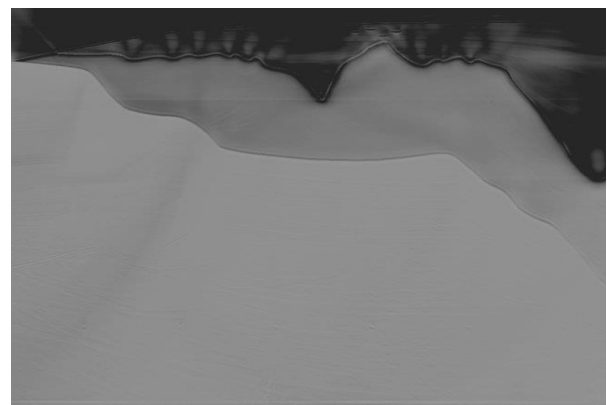


Figure 2: Zoomed portion of the gradient kernel (equation 2) for Sigsbee 2d imaged with RTM SWIM.

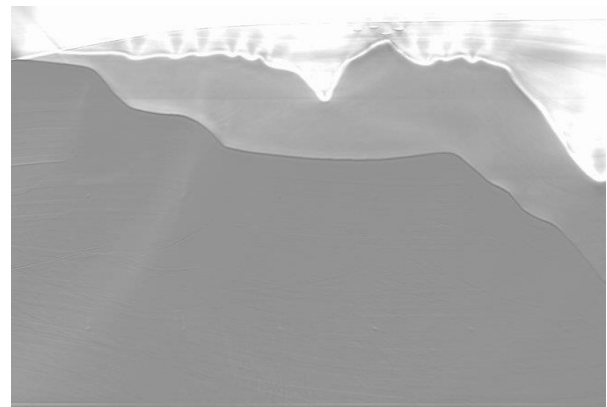


Figure 3: Zoomed portion of the time derivative kernel (equation 3) for Sigsbee 2d imaged with RTM SWIM.

Deconvolution ISIC

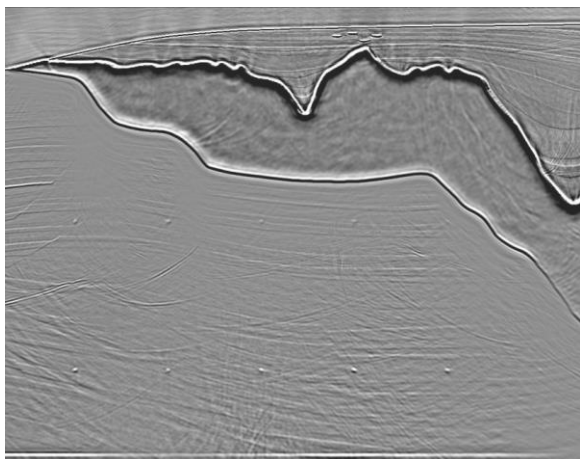


Figure 4: Zoomed portion of the complete deconvolution ISIC image for Sigsbee 2d imaged with multiples.

Figure 4 is comparable to an image obtained from standard RTM of primaries, but somewhat noisier due to crosstalk between different orders of events (Lu et al., 2011).

Field data example

Figures 5 and 6 show a small section of a 3D wide azimuth surface seismic survey. Figure 5 is imaged using ISIC and primary events, and Figure 6 is a SWIM image using the new deconvolution ISIC imaging condition. Deconvolution SWIM imaging produces an image which is somewhat comparable to the primary image, but enhanced in some important ways. These are expected based on experience with one-way SWIM (Lu et al., 2014).

Density of virtual sources, combined with illumination compensation and spectral whitening, cause the

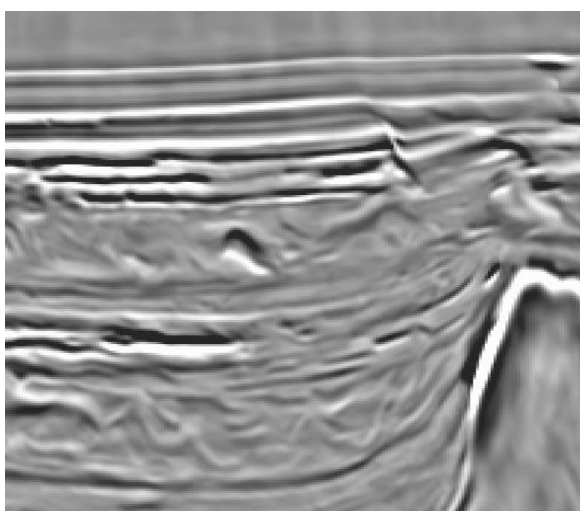


Figure 5: Zoomed portion of Gulf of Mexico RTM.

deconvolution image in Figure 6 to have higher resolution in many of the sediment areas. However, it is also somewhat noisier due to crosstalk between mismatched orders of events and small values in the denominator. For example, see the noise events parallel to the salt, near the center of the figure.

Figures 7 and 8 show shallow depth slices of the same images. The acquisition footprint is visible in the standard RTM, and suppressed by SWIM. Also, the additional area imaged with SWIM can be seen. Some small features appear to be imaged in the RTM result (Figure 7) and not in the deconvolution result (Figure 8). However, this is really just because the deconvolution result is more focused, and these small events appear in a smaller range of depths. The standard RTM result has them spread over a larger number of depth samples.

Conclusions

We extended the inverse scattering imaging condition (ISIC) to the frequency domain in order to implement an RTM deconvolution imaging condition free from low-wavenumber backscatter artifacts. The deconvolution imaging condition balances amplitudes and improves illumination. It also removes the wavelet, enhancing resolution. This combination of deconvolution and backscatter suppression helps RTM SWIM produce quality high-resolution images.

Acknowledgements

The authors thank PGS for permission to publish this abstract, and use the Gulf of Mexico streamer data.

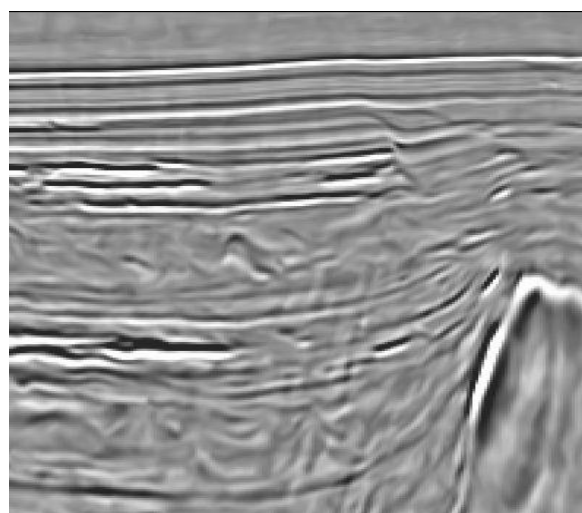


Figure 6: Zoomed portion of Gulf of Mexico RTM imaged with deconvolution ISIC and SWIM.

Deconvolution ISIC



Figure 7: Depth slice of portion of a Gulf of Mexico dataset, imaged with RTM.



Figure 8: Depth slice of portion of a Gulf of Mexico dataset, imaged with RTM using SWIM and deconvolution ISIC.

REFERENCES

- Guitton, A., A. Valenciano, D. Bevc, and J. Claerbout, 2007, Smoothing imaging condition for shot-profile migration: *Geophysics*, **72**, no. 3, S149–S154, <https://doi.org/10.1190/1.2712113>.
- Poole, T. L., A. Curtis, J. O. Robertsson, and D.-J. van Manen, 2010, Deconvolution imaging conditions and cross-talk suppression: *Geophysics*, **75**, no. 6, W1–W12, <https://doi.org/10.1190/1.3493638>.
- Shaoping, L., N. D. Whitmore, A. A. Valenciano, and N. Chemingui, 2011, Imaging of primaries and multiples with 3D SEAM synthetic: 81st Annual International Meeting, SEG, Expanded Abstracts, 3217–3221, <https://doi.org/10.1190/1.3627864>.
- Shaoping, L., N. D. Whitmore, A. A. Valenciano, and N. Chemingui, 2014, Illumination from 3D imaging of multiples: An analysis in the angle domain: 84th Annual International Meeting, SEG, Expanded Abstracts, 3930–3934, <https://doi.org/10.1190/segam2014-0852.1>.
- Stolk, C. C., M. V. de Hoop, and T. Op't Root, 2009, Linearized inverse scattering based on seismic reverse-time migration: Proceedings of the Project Review, Geo-Mathematical Imaging Group, 91–108.
- Valenciano, A. A., S. Crawley, E. Klochikhina, N. Chemingui, S. Lu, and D. N. Whitmore, 2014, Imaging complex structures with separated up- and down-going wavefields: 84th Annual International Meeting, SEG, Expanded Abstracts, 3941–3945, <https://doi.org/10.1190/segam2014-1145.1>.
- Wang, S., M. V. de Hoop, and J. Xia, 2010, Acoustic inverse scattering via Helmholtz operator factorization and optimization: *Journal of Computational Physics*, **229**, 8445–8462, <https://doi.org/10.1016/j.jcp.2010.07.027>.
- Whitmore, N. D., and S. Crawley, 2012, Applications of RTM inverse scattering imaging conditions: 82nd Annual International Meeting, SEG, Expanded Abstracts, 1–6, <https://doi.org/10.1190/segam2012-0779.1>.
- Whitmore, N. D., A. A. Valenciano, W. Sollner, and S. Lu, 2010, Imaging of primaries and multiples using a dual-sensor towed streamer: 80th Annual International Meeting, SEG, Expanded Abstracts, 3187–3192, <https://doi.org/10.1190/1.3513508>.
- Yoon, K., K. J. Marfurt, and W. Starr, 2004, Challenges in reverse-time migration: 74th Annual International Meeting, SEG, Expanded Abstracts, 1057–1060, <https://doi.org/10.1190/1.1851068>.